THE ASTROPHYSICAL JOURNAL, 277:513–525, 1984 February 15

OPTICAL PROPERTIES OF THE KNOTS IN NGC 7385

S. M. SIMKIN[1,2]
Michigan State University
G. V. BICKNELL
Mount Stromlo and Siding Spring Observatory
AND
A. BOSMA
University of Leiden
Received 1983 January 31; accepted 1983 August 4

ABSTRACT

Direct photography and digital spectrophotometry have been used to study the blue optical knots associated with the distorted northeast radio jet in NGC 7385. There are at least two emission patches, aligned with the edge of the jet where the gradient in radio flux is steepest. We have obtained absolute flux measurements of weak emission lines of [O II], [O III], H I, and [S II] and the relatively strong blue continuum coming from these patches. These observations suggest that the material in the knots is metal poor (and thus does not come from the nucleus). The knots are probably interacting with the radio jet, but their exact excitation mechanism and the source of their continuum is uncertain.

Subject headings: galaxies: individual — galaxies: jets — galaxies: structure — nebulae: H II regions

I. INTRODUCTION

It has long been apparent that observations of any optical features associated with the radio-emitting plasma in a radio galaxy can supply more detailed information about the physical conditions in this plasma than can radio observations alone. However, such optical features have been difficult to find. Those which have been discovered appear to be wisps and knots associated only with the most intense areas of radio emission (cf. Blanco *et al.* 1975; references in Simkin and Ekers 1979, hereafter S&E; and van Breugel and Heckman 1982).

These "optical tracers" appear to fall into three categories. (i) Near the nuclei of some radio galaxies, there appear to be different regions of ionized plasma with different excitation conditions which are almost unresolved spatially but which can be identified by means of their different systemic velocities (cf. Simkin 1979; Miley *et al.* 1981; and Ekers and Simkin 1983). This phenomenon is similar to one seen near the nuclei of some Seyfert galaxies (Walker 1968; Ulrich 1983). (ii) Next, just outside the nuclear regions of some radio galaxies, there occur optical jets or knots which seem to be emitting primarily optical synchrotron radiation (Butcher, van Breugel, and Miley 1980). (iii) Finally, in the outer regions of some associated optical galaxies, knots are found which have optical emission lines as well as an underlying optical continuum (Osmer 1978; S&E; and references in van Breugel and Heckman 1982). These objects are extremely faint and difficult to study optically.

Various scenarios have been devised to account for this latter class of optical objects. Most of these evoke interaction between the radio-emitting material and gas or clouds of gas and dust in the nonnuclear regions of the galaxy or intergalactic medium, either forming stars (Osmer 1978; DeYoung 1981) or giving rise to shock-excited gas (Graham and Price 1981; Brodie and Bowyer 1982). The optical continuum can be a composite stellar continuum from newly formed stars or optical synchrotron associated with particle acceleration in the nonthermal plasma or simply thermal continuum from an ionized plasma. Correspondingly the emission lines may be excited by photoionization (from either a stellar or a nonthermal continuum) or by shocks.

Regardless of what the precise mechanism is for the creation and excitation of these optically emitting regions, they appear to be in direct physical interaction with the radio plasma, and optical determination of their internal velocities, densities, and excitation conditions can provide some information about the radio plasma itself. Such optical measurements have become possible only recently, since many of the larger optical telescopes have been fitted with faint object spectrographs and reliable, two-dimensional, linear intensity detectors. The data from these in conjunction with high-resolution radio maps from the VLA make it possible to identify precisely the corresponding radio and optical features and measure their optical spectra quantitatively.

One object which appears to be an excellent candidate for this type of study is an optical knot associated with the distorted northeast side of the type I radio source in NGC 7385. This knot is known to have a blue continuum and faint nebular emission lines (S&E). In addition, Hardee, Eilek, and Owen (1980) have shown that it is embedded in the ridge lines of what appears to be a distorted radio "jet." These authors suggested that the knot is the result of a thermal instability arising from the interaction between the radio plasma and the interstellar gas in the galaxy. However, this interpretation leaves at least three features of the optical emission unexplained. (i) It does not specify the emission-line excitation

[1] Guest Investigator, Hale Observatories, 1978–1980.
[2] Visiting Professor, Department of Astronomy, University of Wisconsin, 1982–1983.

mechanism, which in this picture could be either collisional excitation in a cooling gas or shock excitation due to the nonisobaric stages of the thermal instability. (ii) It does not explain the observed blue continuum. (iii) It does not explain the observed redshift of the emission lines in the knot with respect to the galaxy nucleus.

Any discussion of these unanswered questions requires much more complete data than those reported in S&E. At optical wavelengths such data can provide: (i) a measure of the electron density in the emission-line gas, from the [O II] or [S II] lines; (ii) an indication of the presence of internal reddening from dust, by measuring the Balmer decrement; and (iii) a measure of the near-UV continuum from the knots to see if the extrapolated UV flux is sufficient to account for the observed ionized material. In this paper we report measurements of high-dispersion, optical spectra of the optical-radio knot in NGC 7385 which provide firm determinations or upper limits to the physical parameters listed above. In addition, we describe an analysis of the optical structure in the knot which strongly suggest that it is associated with the radio lobe and is not just a chance superposition. These measurements do not unambiguously indicate the precise ionization and excitation mechanisms for the knot, but they do suggest that such an unambiguous determination cannot be done on the basis of optical observations alone.

II. OBSERVATIONS

a) Spatial Structure—Relation to the Radio Continuum

Of crucial importance is the exact spatial relationship between the optically emitting gas and the radio emitting gas in these objects. Since they are only in projection, this relationship can never be determined exactly. However, precise astrometric measurements at both radio and optical wavelengths can resolve much of the ambiguity. The original optical measurements of the knot in NGC 7385 (marked on the map in Hardee, Eilek, and Owen 1980) were measured on a 103aO emulsion taken on the Palomar Schmidt with an ultraviolet filter. This plate-filter combination gives relatively poor images. Thus, to obtain better resolution, three additional plates (on IIIaJ and IIIaF emulsions in the B' and R bandpasses) were taken with the Palomar Schmidt in 1978 June. These were digitized on a PDS microdensitometer and positions of 11 AGK 3 stars and 10 fainter secondary stars within 20′ of NGC 7385 were measured using a numerical centroiding routine. A nine parameter gnomonic fit to these positions was then used to superpose the digitized optical image on the radio contours published by Hardee, Eilek, and Owen (1980). These are shown in Figure 1*a*. The rms errors to the plate solutions for this superposition were less than 0.″22 in both R.A. and decl. The positions of the secondary standards and their residuals are listed in Figure 6 (at the end of § IV) with a finding chart. The absolute astrometric accuracy of the VLA at the time the measurements of Hardee, Eilek, and Owen (1980) were done was not discussed in that paper. Experience suggests, however, that it was probably better than 1″ (J. W. Dreher, private communication).

The optical image shown in Figure 1*a* is from three IIIaJ plates which have been summed digitally. The position of the knot measured by S&E is located at the leading edge of the optical feature in Figure 1*a*. A clearer picture of the relationship between the optical "knot" and the radio structure in this area, however, may be obtained from Figure 1*b*. This shows the results of converting the digitized photographic images to relative intensity and subtracting the symmetrical component of the underlying galaxy image by using the technique described by Butcher, van Breugel, and Miley (1980). In this plot the "knot" shows up as an extended set of at least two "knots" or wisps. Positions of the 10 secondary astrometric standards and the two knots were then measured on this processed image and analyzed in the same way as the original AGK 3 stars. The fit to these positions has an internal error of less than 0.″29 in both R.A. and decl. and yields positions for the knots of

Knot 1: $22^h47^m26^s.121 + 11°20'49''.42$; epoch 1978.6 (ref. to 1950.0)

Knot 2: $22^h47^m26^s.256 + 11°20'51''.91$; epoch 1978.6 (ref. to 1950.0),

where knot 1 is the brighter wisp and knot 2 the fainter. Thus, the features are spread out over a region at least 500 pc in size (3″ at 104 Mpc, with $H = 75$ and $V_r = 7820$ km s^{-1}, see § III*c*).

A more detailed analysis of the optical structure was conducted by subtracting a digitized R image from those at B' (the aforementioned IIIaJ plates). This showed that all of the regions of excess flux (the dark shades in Fig. 1) are bluer than the underlying galaxy. The irregular patch at the head of the southwest jet may be similar to the type of optical structure found by Butcher, van Breugel, and Miley (1980) in other nearby radio galaxies with strong radio jets. (The feature to the SSW is a star.) However, the analysis of Butcher *et al.* was done by using direct intensity images while the results of Figure 2 come from photographic material. The photographic images are heavily saturated near the nucleus and are not as reliable there as in the outskirts of the galaxy where the intensity gradients (sky + galaxy) are not as steep. The spectra (described later) which pass through the blue region to the SW of the nucleus show no unusual features although, again, the brightness of the underlying galaxy in this region would be expected to introduce sufficient photon noise to obliterate any emission lines as faint as those found in the knots to the NE.

b) Spectroscopic Observations

The intensity maps shown in Figure 1*a* and *b* were used to set up the slit positions for the spectroscopic observations. The slit was set at P.A. 61° through the nucleus and at P.A. 49°, 2.″2 south of the nucleus (Fig. 1*c*). This latter position was used for most of the observations. (The slit was also set in P.A. 62° for two runs but these measurements were not reduced because they were taken in such poor seeing.) The slit width was set at 1.″83. Comparison of Figure 1*c* with Figure 1*b* shows that both knots were included along the slit.

The object was observed for a total of 4.7 hr on two successive nights (1980 August 16/17 and 17/18) with the image photon counting system (IPCS) on the Cassegrain (RGO) spectrograph of the Anglo-Australian Telescope (AAT). These observations are summarized in Table 1. Three different combinations of gratings and grating angles were used to give coverage at ~0.5 Å/pixel over a range of 3500–5300 Å and

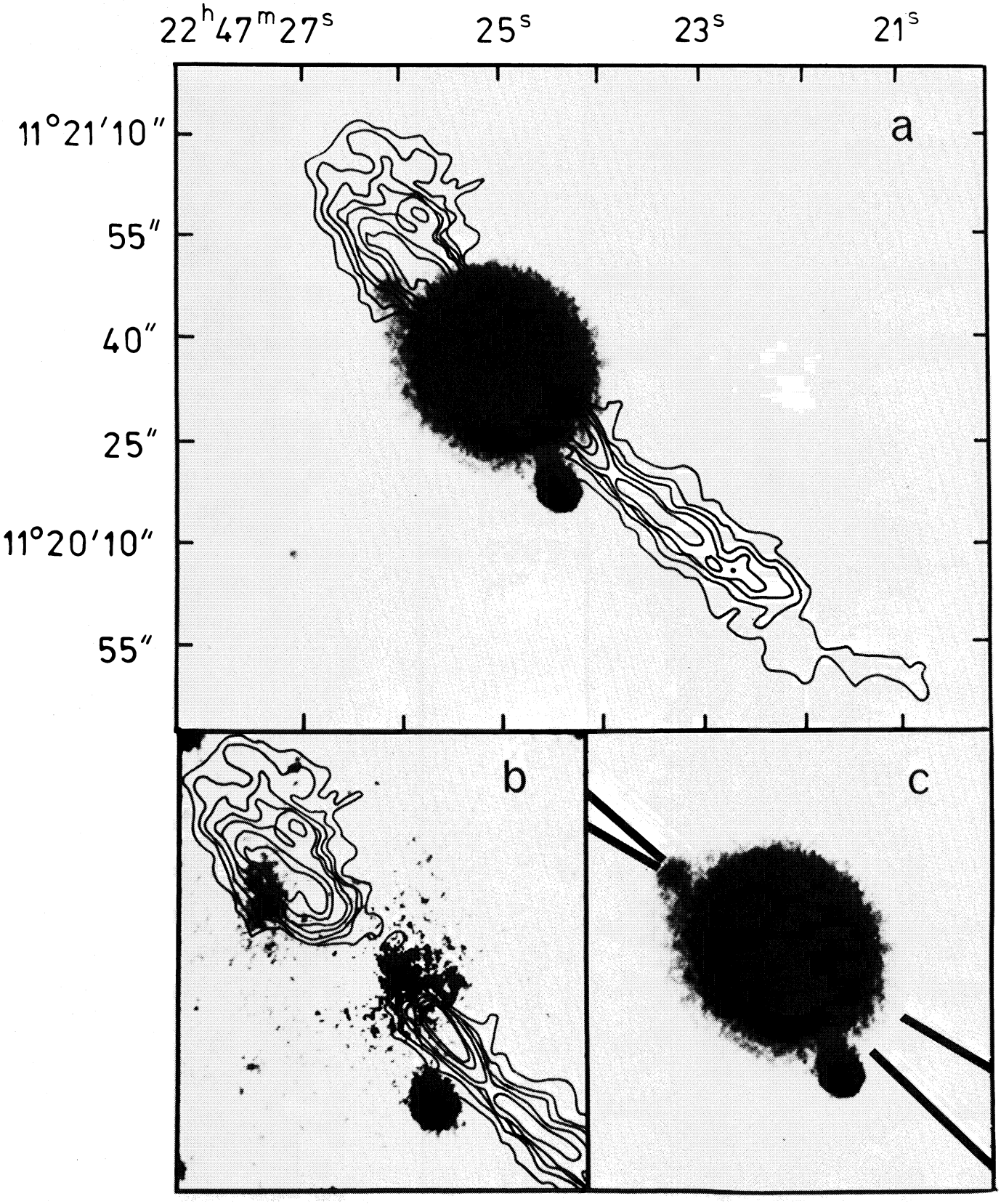

FIG. 1.—NGC 7385. (*a*) Radio contours on the optical image; (*b*) radio contours on the regions of optical excess (object to South of contours is a saturated star image); (*c*) spectrograph slit positions.

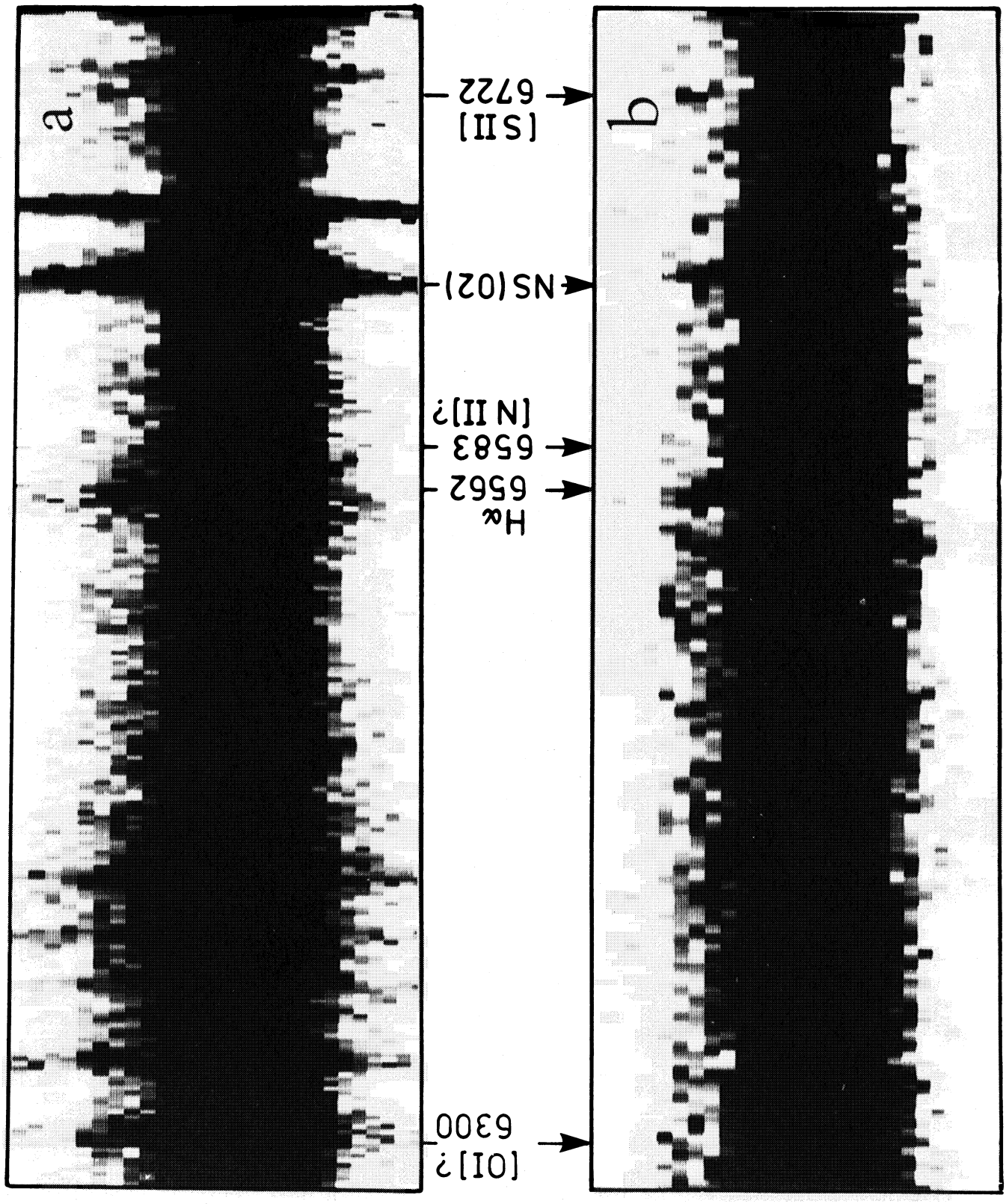

FIG. 2a.—Low-dispersion red spectrum corrected for wavelength distortion. (*b*) Same as 2*a* but with sky subtracted.

TABLE 1

IPCS OBSERVATIONS OF NGC 7385

Run Number	Zenith Distance star	Slit Position (° N of E)	Exposure (s)	Range (Å)	Dispersion (Å per pixel)
18	59°3	61	1500	3450–4500	0.5
19	55.0	61	1500	3450–4500	0.5
23	49.3	242	1000	3450–4500	0.5
38	44.6	242	200	3450–4500	0.5
43	50.3	229	2000	3450–4500	0.5
45	55.5	229	1000	3450–4500	0.5
80	44.7	229	2000	3600–7200	2.1
82	48.9	229	2000	3600–7200	2.1
84	55.1	229	2000	4300–5300	0.5
86	60.3	229	1870	4300–5300	0.5

2.1 Å/pixel over 3600–7200 Å (Table 1). Because poor seeing forced us to repeat two of the runs (23 and 38), we were not able to obtain optimum measurements with the low-dispersion grating. We deemed it important to observe the continuum between 4000 and 4600 Å to ensure a match between our two sets of high-dispersion measurements. Thus, the 3600–7200 Å observations were taken without a blue filter (which cuts off sharply in the 4000–4600 Å region and might have distorted this measurement). This allowed the second-order blue (3050–3600 Å) in the spectrum to overlap the first-order, long wavelength, red region (from approximately 6100 Å onward). We were able to correct for this "blue leak" by using measurements of standard stars with and without a blue filter. However, the blue contamination of the red spectrum seriously deteriorated the signal-to-noise ratio, particularly in the regions where the night sky spectrum contains strong UV emission bands (see Figs. 2*a* and 3*c* for examples).

The IPCS format was set to cover approximately 185″ along the slit, allowing the sky background intensity to be measured simultaneously with that of the knots. The slit (see above) projected onto the image plane corresponded to approximately 3 pixels for all dispersions.

A portion of one of the low-dispersion spectra, corrected for wavelength-position distortion, is reproduced in Figure 2*a*. The same frame, with the sky spectrum subtracted, is shown in Figure 2*b*. (The video display in these reproductions covers only a small portion of the full dynamical range in the original spectra.)

Both nights were photometric. The seeing was variable and poor in the middle of both nights (3–5″) and better (1–2″) for the three hours after sunset and before sunrise. This poor seeing combined with refraction effects appears to be the principal source of error in our absolute flux determinations (§ II*c*).

c) *Spectroscopic Reductions*

The data were reduced using full two-dimensional programs on the VAX 11-780 computers at MSSO, KPNO (Wide Field Camera Team VAX), and MADRAF (Madison, WI). These programs were written as a collaborative effort by A. J. Pickles, S. M. Simkin, A. Bosma, D. Warne, G. Quinn, and the computing staff of MSSO. They are described in detail in Simkin *et al.* (1983).

Arc calibration spectra were taken both before and after each galaxy observation and were used to calibrate the galaxy spectra in wavelength, correcting for "S" distortion along the slit (cf. Fig. 2*a*). This correction was reliable to approximately 0.1 Å for the high-dispersion spectra and 0.4 Å for the low-dispersion spectra. Thus, the sky subtraction for the low-dispersion spectra is not as good, and (in the region of strong night sky lines) this is one of the principal sources of error in our measurements of emission-line fluxes redder than 5300 Å.

Flux calibrations were based on observations of three white dwarf stars calibrated by Oke (1974). The same slit size was maintained while observing the standard stars, and an attempt was made to observe them at approximately the same air mass and slit position relative to the local hour circle as the corresponding galaxy observations. The standards were observed through neutral density filters. The errors in correction for these filters are negligible compared with those inherent in the data themselves. However, an added uncertainty was introduced into the measurements because the filters were labeled incorrectly in the spectrograph. This ambiguity seems to have been satisfactorily resolved *a posteriori* since where they overlap in wavelength, the final flux calibrations agree to within the measurement errors (an incorrect match would produce at least a factor of 2 in the final calibrated intensities from different wavelength regions). Standard extinction coefficients were used in the flux calibrations except in the region of the atmospheric "*B*" band, where some attempt was made to partly correct for this molecular feature. (This correction was *less* than the actual extinction in this feature, as can be seen in the sky-subtracted spectrum in Fig. 3*c*).

The low-dispersion spectra were observed with the slit P.A. nearly parallel to the local hour circle, and differential refraction had the effect of dispersing the light *along* the slit for these observations (creating a type of "S" distortion in wavelength). The high-dispersion spectra were corrected for this "S" distortion, but because the low-dispersion spectra had first-order red and second-order blue intensities superposed, they could not be corrected for this effect. Thus, refraction is also a significant source of error in the flux calibrations for the low-dispersion spectra below 4000 Å and above 6800 Å (Fig. 4*b*).

The flux calibration procedure assumes that the observed flux has the same spatial distribution as that of the comparison star (i.e., a point spread function). Neither the observing conditions (poor seeing) nor the available information about source geometry (the brighter knot was found to be consistent with a point source by S&E) warranted a more complex correction and none was attempted.

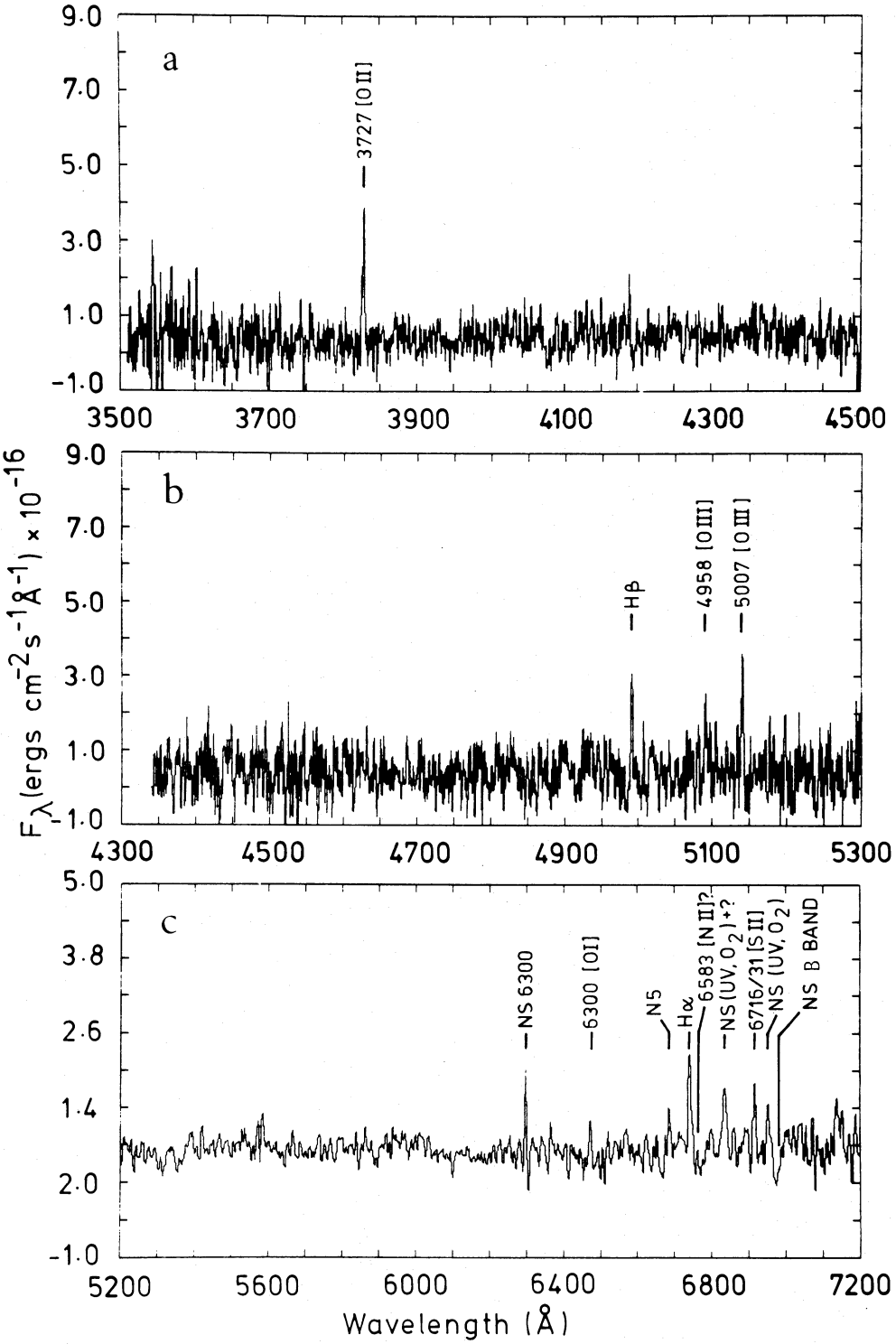

FIG. 3.—Flux calibrated emission line spectra. (*a*) UV; (*b*) blue-green; (*c*) red (low-dispersion).

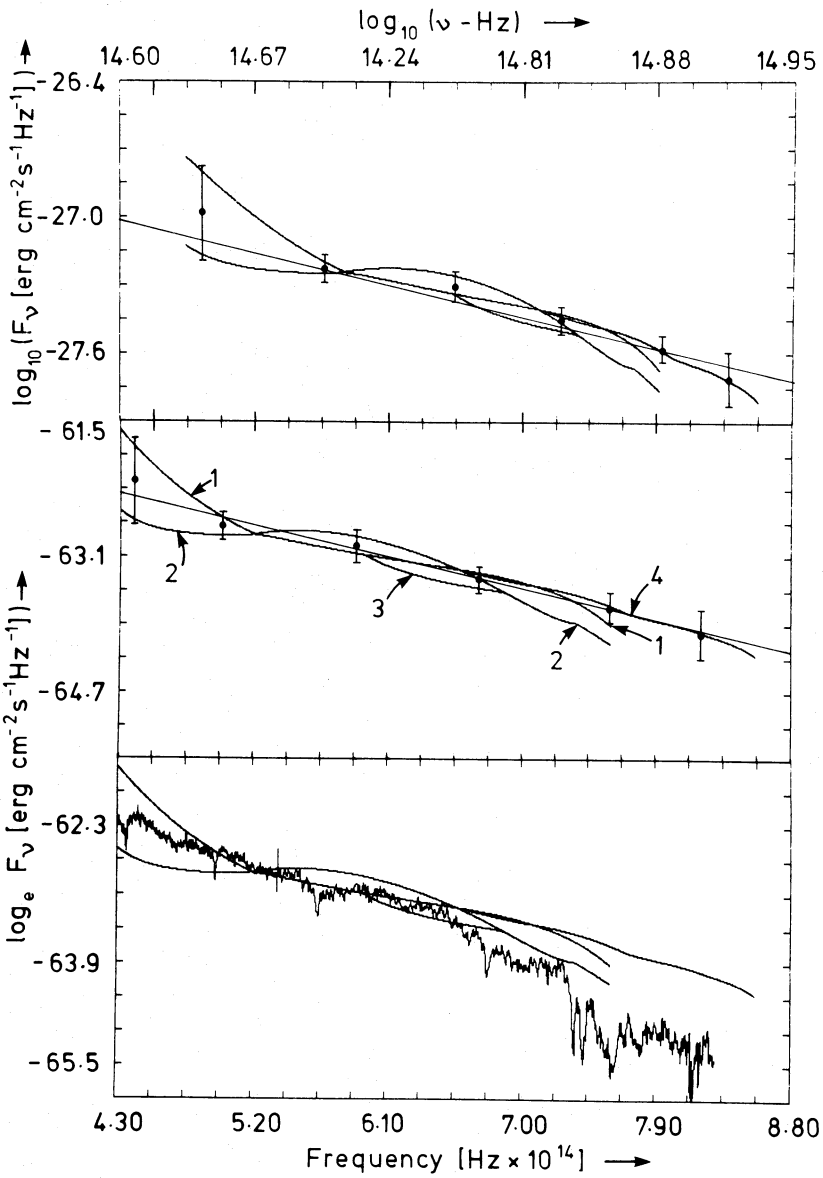

FIG. 4.—Continuum flux from the knot, bars indicate errors. (*a*) Log *Fv* vs. log *v*; (*b*) ln *Fv* vs. *v*; (*c*) same as *b* but with nuclear spectrum superposed.

The accuracy of the absolute flux calibration can be estimated by comparing different observations of the same standard stars. These agreed to between 0.01 mag (1%) at 3500 Å and 0.08 mag (8%) at 4150 Å for the high-dispersion blue observations, 0.12 mag (4300–5300 Å) for the high-dispersion green observations, and 0.072 mag (3650 Å) to 0.25 mag (6800 Å) for the low-dispersion measurements. As noted above, the principal errors in the red were dictated by the uncertainty in the blue leak correction and the intrinsic low sensitivity of the IPCS in the red. Errors in the blue and green high-dispersion fluxes are most likely due to variations in seeing and refraction (particularly for the green, which was done at an air mass greater than 1.6).

III. ANALYSIS

Because the object is extremely faint and superposed on the light from the outskirts of NGC 7385, different techniques were used to obtain the flux in the lines and that from the continuum.

a) Emission-Line Fluxes

For the emission-line measurements, it was most important to obtain good subtraction of the night sky lines and the underlying galaxy spectrum absorption lines. The wavelength calibrations are most closely matched for spectral rows which are adjacent. Thus, night sky spectra from those sky rows nearest the knots were subtracted from the knot spectrum. Similarly, the underlying galaxy spectrum for the region of the knots was calculated by weighting the galaxy spectrum from rows on either side of the knot by the ratio of the total intensity of the galaxy underneath the knot to that on either side (derived from a radial intensity profile through the knot). Finally, the "blue leak" in the red region of the low-dispersion spectrum was removed only for the underlying

TABLE 2

EMISSION-LINE FLUXES

Rest Wavelength (Å)	Flux (ergs cm^{-2} s^{-1} × 10^{16})
3726.1 [O II]	3.2–4.6
3728.8 [O II]	6.3–7.5
3727 (sum)	9.6–11.6
4862 (Hβ)	6.7–7.5
5007 [O III]	8.0–9.3

continuum (since no detailed measurements of the spectrum between 3100 and 3500 Å were available and the observed UV continuum had to be extrapolated to make the correction). Thus, as noted before, the noise in the red part of the low-dispersion spectra was greatly increased by the underlying UV night sky lines. The resulting flux calibrated spectra are shown in Figure 3.

The emission-line positions were measured using a weighted centroiding algorithm. The emission-line fluxes were then determined by fitting a straight line to the continuum on either side of the measured line position, varying the interval of this fit between 10 and 80 Å, and summing the flux in the emission line in excess of this fitted continuum. The different fluxes measured in this way gave mean values (for any one wavelength) which were consistent with the underlying continuum "noise" as calculated in the continuum fitting procedure.

When identifying emission lines on the low-dispersion spectra, particular emphasis was placed on using the full-slit spectra prior to sky subtraction. This technique is a much more reliable method for differentiating between true emission lines and the artifacts introduced by incomplete sky subtraction than the more customary intensity-wavelength plots (such as Fig. 3*c*).

The measured fluxes for the stronger lines are given in Table 2. The line ratios for both these and the weaker lines are given in Table 3. The range in values given for each line represent the maximum (2 σ) error expected from any one of the several sources discussed in § II*c*. The weak line ratios have been given *only* as a range in values to emphasize that any one value can be distorted by poor sky subtraction (because of irregularities in the wavelength calibration). For example, while the ratio of the mean values for [N II] and [O I] is 0.46, the possible range in this ratio is 0.10–1.3, and it is this range which must be considered in any valid comparison with model predictions.

TABLE 3

EMISSION-LINE RATIOS

Lines	Ratio	log (ratio)
3728/3726 [O II]	1.37–2.34	...
6562/4862 Hα/Hβ	1.85–3.65	...
3727/5007 [O II]/[O III]	1.28–1.45	+0.11– 0.16
5007/4862 (N I)/H β	1.07–1.39	+0.03– 0.14
6583/6562 [N II]/Hα	0.02–0.12	−1.64– −0.73
6300/6562 [O I]/Hα	0.09–0.22	−1.05– −0.67
6300/5007 [O I]/[O III]	0.18–0.44	−0.72– −0.36
6722/6562 [S II]/Hα	0.27–0.80	−0.57– −0.10

For the lines measured on the high-dispersion spectra, the dominant error appears to arise from photon noise in the underlying galaxy and night sky spectrum. For Hα it comes from the flux calibration. For the weak lines in the low-dispersion spectra ([O I], [N II], and [S II]), the dominant source of "noise" is incomplete subtraction of the underlying UV night sky emission lines. The [N II] line in particular is unusually weak and the value given in Table 2 may be only an upper limit.

b) Continuum Fluxes

To determine the galaxy plus sky spectrum underlying that of the knots, the night sky spectrum was obtained by averaging over all usable rows corresponding to positions greater than 70″ from the nucleus of the galaxy (corrected for vignetting). Then the galaxy spectrum corresponding to positions on the opposite side of the galaxy from the knots was determined by summing over all rows symmetrical to those containing the knots' spectrum. These were added together (weighting the night sky averages by the number of rows in the knot spectra) and subtracted from the total measured spectrum (raw counts) at the position of the knots. The result of this procedure is a spectrum with higher noise in the region of strong night sky lines but a mean which is more accurate than that of the spectrum used for the line flux measurements. The mean continuum at any one position was then determined by fitting a series of third- to seventh-order polynomials to the resultant measured counts over 300–500 channels. These polynomials were then spliced together where they overlapped to produce the final "best" fit to the raw data. This best fit was calibrated to absolute flux. The results are shown in Figure 4, with the error bars in Figure 4*b* indicating the errors in the flux calibration (see § II*c*). In Figure 4*c* the knot's continuum and the nuclear spectrum (scaled to agree with that of the knot at 7500 Å) have been plotted together as ln Fv versus v. The knot is clearly bluer than the galaxy nucleus.

Both power-law spectra and exponential synchrotron spectra are associated with radio continuum sources and are often evoked to describe the "blue" component in the optical spectra of these objects. To test their applicability here, we have fitted straight lines to the continuum measurements in both the (log Fv, log v) (Fig. 4*a*) and (ln Fv, v)-planes (Fig. 4*b*).

Both plots can be fitted to within the errors, giving

$$Fv \approx 130 \times v^{-2} \text{ ergs cm}^{-2} \text{ (sHz)}^{-1} \quad (1)$$

for log Fv versus log v in the optical region, with the variance on the spectral index being $\alpha = 2.00 \pm 0.25$. And

$$Fv \approx 4.41 \times 10^{-27} \exp(-v/2.5 \times 10^{14}) \text{ ergs cm}^{-2} \text{ (sHz)}^{-1} \quad (2)$$

for ln Fv versus v. A straight line is a slightly better fit to the (ln Fv, v) plot.

Convolution of the calibrated continuum measurements with standard UBV filter responses gives $V = 20.4 \pm 0.2$ mag, $U-B = -0.46 \pm 0.15$, and $B-V = 0.58 \pm 0.15$. Comparison of these measurements with corresponding values reported in S&E shows that the emission-line fluxes from the stronger lines are a factor of 1.3 to 2.2 greater in the present data (the weaker lines were not measured by S&E). Similarly, the

continuum measurements at 6.6×10^{14} Hz are a factor of 1.7 to 3.5 greater here. These differences are not surprising in view of the fact that the present measurements were done with a wider entrance slit oriented *along* the knots, while the earlier measurements were done only through the one knot closest to the nucleus of NGC 7385.

c) *Systemic and Internal Velocities of the Ionized Gas*

The positions of the emission lines in the calibrated, high-dispersion, blue spectra were measured using a numerical centroiding technique. The resulting redshift for the gas in the brighter knot was $\Delta\lambda/\lambda = 0.0266 \pm 0.00013$. The group velocity of the stars in the galaxy located along the slit, 4″–8″ to the southwest of the knot, was measured by cross correlating the blue, high-dispersion galaxy spectra in this region with those of the nucleus. The redshift of the nucleus was then obtained by measuring the cores of the H and K absorption lines in the nuclear spectra (giving 7820 km s^{-1} as noted earlier). The resulting stellar redshift was $\Delta\lambda/\lambda = 0.0258 \pm 0.00021$. The measured redshifts of the emission lines and adjacent stellar spectra (§ III*c* above) give a velocity difference of 230 ± 70 km s^{-1} between the knot and the surrounding galaxy. This is very similar to the difference of 330 ± 150 km s^{-1} between the galaxy nucleus and the knot found earlier by S&E.

The emission-line widths in the λ5007 and Hβ lines are not appreciably wider than those in the comparison spectrum. There is not sufficient broadening present to warrant a detailed line-width analysis even for the high-dispersion spectra where the unblended comparison lines fall in three pixels or less. It is clear, however, that any broadening of Hβ or λ5007 greater than the instrumental width would be notable. Thus, we conclude that the internal velocities in the ionized gas are less than 60–90 km s^{-1}.

IV. DISCUSSION

The distortion of the radio ridge lines around the two patches of nebulosity (Fig. 1*b*) strongly suggests that interaction between the jet and two clouds may be responsible for the emission lines and associated continuum. However, this spatial coincidence does not completely rule out the possibility that the knots are simply the chance superposition of an isolated extragalactic H II region on the outskirts of NGC 7385. If interaction between interstellar gas and the radio plasma is responsible for the knots, then, as outlined in the Introduction, there are several different mechanisms possible for the production of the observed emission-line nebulosity and continuum. Among these are (i) the jet has entrained a cloud of thermal gas and initiated star formation, producing gas which has been photoionized by early-type stars an an early-type continuum; (ii) the jet has shocked an interstellar cloud producing shock excited lines and blue optical synchrotron emission in the surrounding nonthermal plasma; (iii) a strong bow shock has been formed by the supersonic flow of the radio jet around a cloud and the ultraviolet synchrotron emission from this shock has photoionized the cloud (see Blandford and Königl 1979); (iv) the jet has initiated a thermal instability in the interstellar medium (Hardee, Eilek, and Owen 1980). These different scenarios predict that the continuum from the knots will be stellar, synchrotron (exponential or power-law), or thermal, respectively, while the ionization will be caused by photoionization (from either a hot stellar or synchrotron continuum), shock heating, or heating by a thermal instability.

Because the knots are on the outskirts of a galaxy where the underlying stellar contribution is small, we believe that the present measurements are far better than much of the available data for many weak emission-line galaxy nuclei which are 4 to 5 mag brighter (cf. the recent discussion by Keel and Miller 1983). Despite this, neither the data nor the existing theoretical models of emission-line objects are extensive enough to unambiguously decide between the above alternatives. However, the emission-line fluxes and ratios, the shape of the optical continuum, and the redshift, 230 km s^{-1}, of the emission lines with respect to the surrounding stars in the galaxy all impose important constraints on the assumptions in these different pictures. These constraints and their implications are described in the following discussion.

a) *Emission-Line Fluxes and Ratios*

The data in Tables 2 and 3 provide information about the density and mass of the ionized gas, its internal reddening, and possibly its metal abundance and the nature of its excitation mechanism.

i) *Electron Density in the Ionized Gas*

An upper limit on the local electron density, N_e, of approximately 100 cm^{-3} is implied by the [O II] 3728, 3726 ratio of 1.37 to 2.34. A lower limit can be obtained by assuming the gas to be in pressure equilibrium with the radio plasma. For a minimum nonthermal pressure of 5.5×10^{-12} dynes cm^{-2} (Hardee, Eilek, and Owen 1980) and a thermal temperature of $T \approx 10^4$, N_e will be greater than or equal to 2 cm^{-3}.

ii) *Flux from* Hβ

The value of $f(\beta) = 6.7$ to 7.5×10^{-16} ergs cm^{-2} s^{-1} (Table 2) can be used to derive the filling factor and mass of the ionized gas and establish some constraints on the type of continuum which might be responsible for the excitation.

The mass of ionized gas observed, M_g, can be determined from the Hβ flux and the electron density as

$$M_g = [L(\beta)/(h\nu\alpha_\beta^{\rm eff} N_e^2)] \times N_e M_H , \qquad (3)$$

where the quantity in square brackets is the effective volume of the emitting plasma. For an Hβ emissivity coefficient, $\alpha_\beta^{\rm eff}$, of 3×10^{-14} cm^3 s^{-1} and at a distance of 104 Mpc (based upon a redshift of 7820 km s^{-1}, § III*c*, and a Hubble constant of 75 km s^{-1} Mpc^{-1}), the lower limit on N_e then gives $M_g \approx 3.4 \times 10^6\ M_\odot$ while the upper limit gives $M_g \approx 6.3 \times 10^4\ M_\odot$, and the effective volumes are 2×10^{63} cm^3, and 7.5×10^{59} cm^3, respectively. These latter values, combined with the *projected* scale of $\sim$500 pc between the knots (§ II*a*) yields a "filling factor" of $\sim 10^{-1}$ to $\sim 10^{-5}$, reinforcing the impression noted earlier (S&E) that the knots are unresolved.

A population of hot stars of types earlier than B1 could produce the ionized hydrogen and still be consistent with the observed optical continuum. On a more empirical tack, the observed ratio of the flux in Hβ to the flux in the continuum at V (5.5×10^{14} Hz) is similar to that found for at least half the narrow-line, extragalactic objects studied by Neugebauer

et al. (1976) which are believed to have photoionization by early-type stars as their principal excitation mechanism.

With $fv = 3.6$ to 4.0×10^{-28} ergs cm^{-2} (sHz)$^{-1}$ at Hβ (from the continuum fits in § II*b*), the equivalent width of Hβ is 14 to 18 Å. This low value immediately rules out thermal recombination as a source for the continuum since the expected value of W(Hβ) for a recombination continuum is on the order of 1000 Å (from the values in Osterbrock 1974, p. 104).

This Hβ width *is* consistent with the observed continuum as the source of ionization (if a power law). In this case, if the gas absorbs most of the ionizing UV flux, the expected spectral index, α, for the continuum can be calculated from W(Hβ) using the relationship given by Ferland and Netzer (1983):

$$W(\mathrm{H}\beta) \approx 560 \times \alpha^{-1}(\tfrac{3}{16})^{\alpha} \text{ Å} . \quad (4)$$

The observed equivalent width for Hβ implies $\alpha = 1.73$ to 1.84, which is within the measured slope for the optical region (§ III*c*).

iii) Hα/Hβ

At a galactic latitude of −41°.3 the foreground absorption in V for NGC 7385 should be less than 0.07 mag (from Sandage 1973). This will alter the Hα/Hβ ratio by less than 3% (cf. the reddening ratios for Hα/Hβ in Osterbrock 1974, p. 171). The ratio of 1.85 to 3.65 for Hα/Hβ brackets the classical "case B" value for radiative recombination (2.74 to 3.03 at $N_e = 10^2$), (cf. Osterbrock 1974, p. 69). Thus, within the measured errors there appears to be little intrinsic reddening in the knots themselves. Certainly there is no suggestion of the steep Balmer decrement observed in many active galaxy nuclei.

iv) *The Line Ratios*

Until recently, it was believed that there were several distinguishable differences between the optical emission-line spectrum of a shock-heated gas and that of a gas photoionized by a power-law spectrum (cf. the references in Baldwin, Phillips, and Terlevich 1981, hereafter BPT). More detailed models of gas clouds photoionized by dilute, power-law continuum, radiation fields, however, now demonstrate that the situation for the stronger, more easily measured emission lines is ambiguous (cf. Ferland and Netzer 1983 and Halpern and Steiner 1983). In spite of this, there are some tentative conclusions which can be drawn from the present emission-line data.

For this discussion we represent our measured line ratios in terms of the diagrams developed by BPT because they provide a good, *empirical*, diagnostic tool. They encompass a variety of different observed objects. In addition, the empirical data represented in their diagrams have been corrected for internal reddening, and the observed ratio of Hα/Hβ for the knots in NGC 7385 suggests that it is much more appropriate to compare the present data with such dereddened measurements. Thus, in Figure 5, our measured line ratios are plotted in order of increasing estimated error (*a* through *d*) with the single-hatched regions indicating the loci of the low-excitation objects identified by BPT, the cross-hatched regions indicating the high-excitation objects, the blank regions indicating H II regions, and the solid line, the region of "isolated extragalactic H II regions."

At first galance, our present measurements are not consistent with any of the objects described by BPT (although on the average they lie closest to the very poorly determined "isolated extragalactic H II regions"). The [S II] lines were not included in the BPT analysis and thus are not plotted. The [S II] flux could indicate shock excitation since it is well known that [S II] is a significant component of shock excited spectra (see, e.g., Raymond 1979; Shull and McKee 1979). However, the [S II]/Hα ratio (between 0.27 and 0.80) also brackets the values which are generally found for blue galaxies and isolated extragalactic H II regions (Neugebauer *et al.* 1976; Searle and Sargent 1972; and O'Connell, Thuan, and Goldstein 1978).

v) *Power-Law Photoionization*

Comparison of the plots with the recent, theoretical, power-law models noted above suggests that the line ratios found here *may* be consistent with a low-ionization parameter model with extremely low metal abundance. In particular, the non-abundance dependent ratios of [O I], [O II], and [O III] agree well with the calculations of both Ferland and Netzer (1983) and Halpern and Steiner (1983) for a gas ionized by a very dilute, power-law radiation field. In addition, the [N II]/Hα, [O III]/Hβ, and [O I]/Hα ratios found here are also consistent

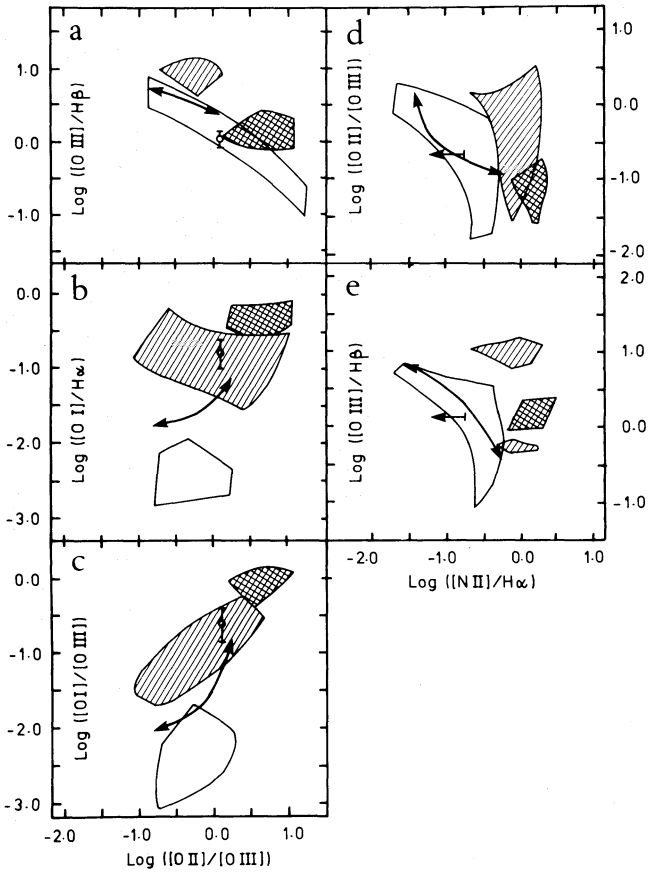

FIG. 5.—The measured line ratios plotted in the BPT plane. *Cross-hatched area:* region of low-excitation objects; *Double cross-hatched:* high-excitation; *Open area:* normal H II regions; *Solid line with arrow heads:* extragalactic H II regions.

with the Ferland and Netzer calculations with an ionization parameter $U = 10^{-3.5}$ but extrapolated to a metal abundance of *less* than 0.1 solar (a very rough estimate suggests ~ 0.06 solar). The fact that both of these models are for much higher N_e than found here (10^3 as opposed to less than 10^2) means that they cannot be applied directly to the present data. The consistent trend toward low metal abundance for all of the abundance-dependent line ratios is, however, very suggestive.

vi) *Shock-Heating*

When comparing the observed line ratios with those expected from a shock-heated gas, the present theoretical picture is even less clear. The value of N_e obtained from the [O II] lines will not be representative of that in the region producing the [O III] lines because these two species will occur predominantly in different regions. In addition, the intrinsic faintness of this object makes it difficult to measure the important [O III] 4363 line (which would give direct information about the [O III] region), or even establish an upper limit on its ratio to 5007 of less than 1:20 (Fig. 3*b*). Furthermore, the upper limit for the emission line widths found in § II*a* implies that any shocks present must have velocities lower than 60–90 km s^{-1}. However, the most recently published models of low-velocity shocks (Shull and McKee 1979) do not cover metal abundances as low as 0.03 solar.

The suggestion of very low metal abundance found by extrapolating the theoretical power-law models discussed above is reinforced by examination of the diagnostic diagrams for shock-heated regions published by Dopita (1977). Although Dopita does not present specific models for low velocity, low metal abundance gas, the effects of metal abundance are presented for low values of N_e. Again, *extrapolation* of Dopita's diagrams suggests a metal abundance of 0.02 to 0.06 solar (see also Dopita, D'Odorico, and Benvenuti, 1980).

vii) *Stellar Photoionization*

Finally, there remains the possibility that the excitation mechanism for the ionized gas is photoionization by hot stars. The strongest evidence against this is the relatively high [O I]/[O II] ratio (Fig. 5*c*). However, as we emphasized in § III*a*, *all* of the faint emission lines beyond 5300 Å suffer from the uncertainties of poor sky subtraction and thus it would be precipitous to hinge the entire discussion on this one line measurement.

viii) *Metal Abundance*

What can be concluded with much more certainty is that the gas in the knots is underabundant in metals. The most striking thing about the spectra in Figures 2 and 3*c* is that the [N II] lines around Hα lie in the noise. In all of the studies referred to above such a low flux for [N II] indicates that the N:H abundance is considerably less than that for the Sun.

One suspects that more extensive models for the emission line spectra of both shock-heated and photoionized gas will be available soon. It is particularly clear that no published results presently exist which directly apply to the low metal abundance, low density case discussed here. In summary, the line ratios seem to give ambiguous information about the *nature* of the ionization mechanism but appear to be consistent with a gas of very low metal abundance.

b) *The Optical Continuum*

Of the various sources for the blue optical continuum suggested by the scenarios cited at the beginning of this section (i. thermal recombination, ii. synchrotron emission, and iii. stellar emission), the first is ruled out by the equivalent width of Hβ [§ IV*a*(ii)].

i) *Synchrotron Continuum*

The situation for synchrotron continuum is complex. It is customary to represent synchrotron emission by a power-law spectrum and, as noted in § III*c*(ii), the equivalent width of Hβ is consistent with photoionization by a source with a spectral index very similar to that observed. If this is the correct representation, the slope cannot be continuous from the radio to the optical since the ratio data of Hardee, Eilek, and Owen, combined with our optical data, give a radio-optical spectral index of approximately 0.4.

In the present case the observed continuum can also be represented by the form $Fv \approx (v/v_c)^{1/2} \exp(-v/v_c)$ (exponential synchrotron) where v_c is the critical frequency of the highest energy electrons in a truncated power law. Then from the exponential fit in equation (2), the critical frequency of the highest energy electrons (the approximate frequency at which the power law would change to an exponential spectrum) is near 2×10^{14} Hz. In this case the radio-IR spectral index should also be approximately 0.4.

Either interpretation of the data implies that particle acceleration is taking place since the radio-optical index is much flatter than the spectral index (0.8) in the rest of the radio plasma (Hardee, Eilek, and Owen 1980). A flat spectral index of 0.5 arises naturally in particle acceleration in shocks (Blandford and Ostriker 1978), while a break in a shock-accelerated spectrum also arises naturally due to cooling of high-energy electrons behind the shock. In fact, Coleman and Bickell (1983) have recently shown that cooling of synchrotron emitting electrons behind the bow shock produced by a jet hitting a cloud gives rise to a change from low to high frequency spectral index of between 1.0 and 1.4. This is similar to the change in spectral index inferred here from our observations.

If the observed optical continuum is exponential synchrotron, however, the gas cannot be ionized by UV photons since these will be insufficient. In this case the gas must be either heated by X-rays (Halpern and Steiner 1983) or shock-excited.

ii) *Stellar Continuum*

Finally, we cannot completely rule out the possibility that the continuum is stellar. We have seen [§ IV*a*(ii)] that the observed Hβ flux is consistent with ionization by a small enough number of early-type stars to leave the optical continuum uninfluenced by their contribution. However, since a typical H II region continuum involves a synthesis of spectral types, it is more realistic to compare the observed continuum with that found in isolated extragalactic H II regions.

One source of comparison is the continuum measurements reported in McCall's (1982) study of extragalactic H II regions. Converting McCall's blue and red color indices to blue and red spectral indices yields blue spectral indices which are flatter than our value of 2.0 (with a few exceptions). The red spectral indices are all flatter than 2.0. A second com-

parison can be made with the continua of the blue galaxies and isolated extragalactic H II regions noted in § IV*a*(iv). Again, these are normally much flatter than the continuum of the knots (with one exception, Markarian 52; Neugebauer *et al.* 1976). Thus the steep continuum observed in the knots is atypical of most extragalactic H II regions but it is not sufficiently atypical that one can rule out an H II region interpretation.

c) *The Emission-Line Redshift with Respect to the Surrounding Galaxy*

If the nebulosity is simply an isolated extragalactic H II region close to NGC 7385, then its redshift of 230 km s^{-1} with respect to the surrounding galaxy is simply due to its motion in the cluster ZW 2247+11. In this interpretation the two nebulous patches might be the result of tidal disruption by NGC 7385. If the nebulosity is due to an interstellar or intergalactic cloud interacting with the northeast jet of NGC 7385 the simplest interpretation of the velocity is that the cloud has been entrained into the jet and is being swept outward at a fraction of the jet velocity (see Blandford and Königl 1979). In any case the observed velocity is inconsistent with the suggestion by Hardee, Eilek, and Owen (1980) that the line emission arises from a thermal instability since by its very nature a thermally unstable cloud is at rest in the interstellar medium. (However, the cloud with which the jet interacts may well have originally formed through a thermal instability in a hot interstellar medium as shown by Hardee *et al.*)

Entrainment of a cloud would naturally lead to shock-excited line emission and optical synchrotron from shock waves in the jet. In this case, the UV synchrotron from the bow-shock would also photoionize the cloud and, as we have already noted [§ IV*a*(ii)], the power-law extrapolation of the continuum can provide enough photons to do this. Thus, one might expect a *mixture* of photoionization and shock excitation in such a situation. However, it would be difficult for an H II region to form under such circumstances since, after the formation of stars, the remaining gas would be swept away by the jet if it had any velocity at all with respect to the cloud.

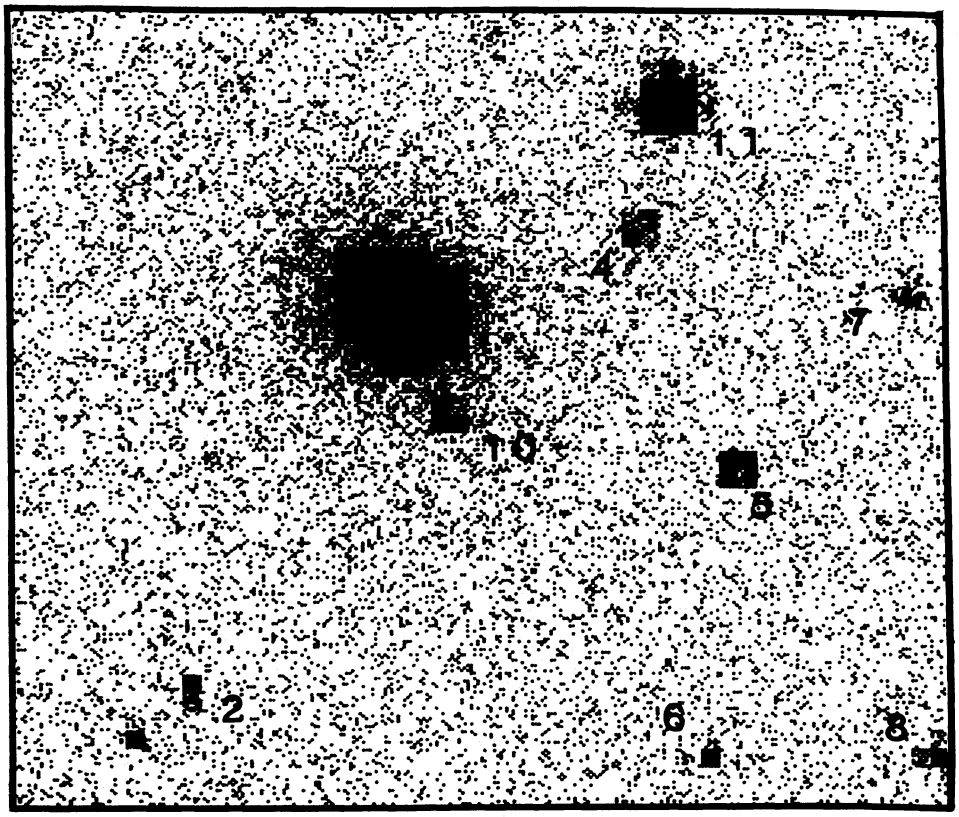

FIG. 6.—Faint stars in the field of NGC 7385 identified by

number,	R.A.,	Δα,	decl.,	Δδ:
(2),	$22^h47^m27^s.442$,	−0″.18,	11°19′27″.65,	−0″.21;
(4),	$22^h47^m22^s.050$,	−0.23,	11°20′51″.26,	+0.29;
(5),	$22^h47^m20^s.981$,	+0.33,	11°20′07″.29,	−0.18;
(6),	$22^h47^m21^s.256$,	−0.27,	11°19′16″.25,	+0.21;
(7),	$22^h47^m18^s.885$,	−0.14,	11°20′40″.32,	+0.07;
(8),	$22^h47^m18^s.611$,	+0.10,	11°19′15″.12,	−0.12;
(10),	$22^h47^m24^s.449$,	+0.50,	11°20′18″.09,	+0.32;
(11),	$22^h47^m21^s.699$,	−0.11,	11°21′13″.62,	−0.38.

V. CONCLUSIONS

The relative positions of the knots and the structure in the radio lobe as well as the systemic velocity of the gas in the knot relative to the stars in the galaxy strongly suggest that the knots are interacting with the radio jet.

The observations presented in this paper tend to rule out the idea that the knots are clouds of gas which have been formed and heated by a thermal instability.

The measured emission-line ratios from the gas in the knot are consistent with photoionization by a power-law continuum. Moreover, the observed Hβ flux and slope of the continuum in the optical also fit in with this interpretation. However, neither shock-heating, nor photoionization by an atypical population of early-type stars can be ruled out by the present observations. In fact, it is possible that both shock-heating *and* photoionization by a power-law continuum are present, as would be the case if a cloud had been entrained by the jet.

All of the different explanations for the line ratios which we have examined agree in pointing to a very low metal abundance for the gas in the knots. This implies that the gas is relatively unprocessed material which was originally associated with the outer regions of NGC 7385 or the intergalactic medium. Thus, the material in the knots was not swept out from the nuclear regions and may have arisen from an accretion flow into NGC 7385.

The knots in NGC 7385 appear to offer a unique opportunity to study gas which is closely associated with radio plasma. They are clearly separated from the nuclear regions and thus relatively uncontaminated by the complex interactions and strong underlying continuum found there. They are, in addition, the only known example of such an object in the outskirts of a galaxy which is close enough to even attempt the type of detailed measurements we have reported on here. Several additional measurements can be done which will help clarify the situation but none of them can be done easily.

i. High-dispersion, optical spectroscopy in the red might conclusively rule out the H II region interpretation by better measurements of the [O I], [N II], and [S II] lines and red continuum relative to Hα.

ii. X-ray and far-UV observations would provide more information about the type of ionizing photons present in the gas.

iii. Finally, high resolution H I observations would provide information about the amount and location of unionized gas associated with the knots. Unfortunately, because of the object's faintness, only the high-dispersion red measurements are feasible with presently available instruments.

We thank L. Binette, D. A. Carter, M. A. Dopita, and I. Wilson for helpful discussions and M. L. McCall for freely making the results of his thesis available to us. S. M. S. is especially grateful to C. R. Lynds for allowing the use of the WFPC Vax and to E. O'Niel for his help with this computer. S. M. S. was a Visiting Fellow at MSSO during the time these observations were made and thanks the director, D. Mathewson, for this support. Partial costs for this paper come from NSF grant PRM-8211851.

REFERENCES

Allen, C. W. 1973, *Astrophysical Quantities*, (3d ed., London: Athlone Press).
Baldwin, J. A., Phillips, M. M., and Terlevich, R., 1981, *Pub. ASP*, **93**, 5 (BPT).
Blanco, V. M., Graham, J. A., Lasker, B. M., and Osmer, P. S. 1975, *Ap. J.* (*Letters*), **198**, 163.
Blandford, R. D., and Königl, A. 1979, *Ap. Letters*, **20**, 15.
Blandford, R. D., and Ostriker, J. P. 1978, *Ap. J.* (*Letters*), **221**, L29.
Brodie, J., and Bowyer, S. 1982, *Bull. AAS*, **14**, 649.
Butcher, H. R., van Breugel, W., and Miley, G. 1980, *Ap. J.*, **235**, 749.
Coleman, C. S., and Bicknell, G. V. 1983, in preparation.
Dopita, M. A., 1977, *Ap. J. Suppl.*, **33**, 437.
Dopita, M. A., D'Odorico, S., and Benvenuti, P. 1980, *Ap. J.*, **236**, 628.
Ekers, R. D., and Simkin, S. M. 1983, *Ap. J.*, **265**, 85.
Ferland, G. J., and Netzer, H. 1983, *Ap. J.*, **264**, 105.
Graham, J. A., and Price, R. M. 1981, *Ap. J.*, **247**, 813.
Halpern, J. P., and Steiner, J. E. 1983, *Ap. J.*, in press.
Hardee, P. E., Eilek, J. A., and Owen, F. N. 1980, *Ap. J.*, **242**, 502.
Keel, W. C., and Miller, J. S. 1983, *Ap. J.* (*Letters*), **266**, L89.
McCall, M. L. 1982, Ph.D thesis, University of Texas at Austin.
Miley, G. K., Heckman, T. M., Butcher, H. R., and Van Breugel, W. J. 1981, *Ap. J.* (*Letters*), **247**, L5.
Neugebauer, G., Becklin, E. E., Oke, J. B., and Searle, L. 1976, *Ap. J.*, **205**, 29.
Oke, J. B. 1974, *Ap. J. Suppl.*, **27**, 21.
Osmer, P. S. 1978, *Ap. J.* (*Letters*), **226**, L79.
Osterbrock, D. E. 1974, *Astrophysics of Gaseous Nebulae* (San Francisco: Freeman).
Raymond, J. C. 1979, *Ap. J. Suppl.*, **39**, 1.
Sandage, A. 1973, *Ap. J.*, **183**, 711.
Searle, L., and Sargent, W. L. W. 1972, *Ap. J.*, **173**, 25.
Shull, J. M., and McKee, C. F. 1979, *Ap. J.*, **227**, 131.
Simkin, S. M. 1979, *Ap. J.*, **234**, 56.
Simkin, S. M., and Ekers, R. D. 1979, *A.J.*, **84**, 56 (S&E).
Simkin, S. M., Pickles, A. J., Bosma, A., Warne, D., and Quinn, G., 1983, "Roo, The Mt. Stromlo Data Reduction Programs," Wisconsin Astrophysics series, University of Wisconsin.
Ulrich, M.-H. 1973, *Ap. J.*, **181**, 51.
van Breugel, W., and Heckman, T. 1982, in *IAU Symposium 97, Extragalactic Radio Sources*, ed. D. S. Heeschen, and C. M. Wade (Dordrecht: Reidel), p. 61.
Walker, M. F. 1968, *Ap. J.*, **151**, 71.

G. V. Bicknell: Mount Stromlo Observatory, P.B. Woden, P.O. 2606, A.C.T., Australia

A. Bosma: Sterrewacht, University of Leiden, 2300 RA Leiden, Netherlands

S. M. Simkin: Department of Physics and Astronomy, Michigan State University, East Lansing, MI 48824